Available online at www.sciencedirect.com
SCIENCE DIRECT
Journal of Nuclear Materials 350 (2006) 56–65
journal of nuclear materials
www.elsevier.com/locate/jnucmat

Analysis of water radiolysis in relation to stress corrosion cracking of stainless steel at high temperatures – Effect of water radiolysis on limiting current densities of anodic and cathodic reactions under irradiation

Kenkichi Ishigure [a,*], Takashi Nukii [a], Shoichi Ono [b]

[a] Saitama Institute of Technology, 1690 Fusaiji, Okabe, Saitama 369-0293, Japan
[b] Institute of Research and Innovation, 1201 Takada, Kashiwa, Chiba 277-0861, Japan

Received 29 June 2005; accepted 12 November 2005

Abstract

Electrochemical corrosion potential (ECP) is an important measure for environmental factor in relation to stress corrosion cracking (SCC) of metal materials. In the case of SCC for in-core materials in nuclear reactors, radiolysis of coolant water decisively controls ECP of metal materials under irradiation. In the previous models for ECP evaluation of stainless steel, radiolysis of reactor water in bulk was considered to calculate the bulk concentrations of the radiolysis products. In this work, the radiolysis not only in bulk but also in the diffusion layer at the interface between stainless steel and bulk water was taken into account in the evaluation of ECP. The calculation results shows that the radiolysis in the diffusion layer give significant effects on the limiting current densities of the redox reactions of the radiolysis products, H_2O_2 and H_2, depending on dose rate, flow rate and water chemistry, and leads to the significant increase in the ECP values in some cases, especially in hydrogen water chemistry conditions.

PACS: 82.45.Bb; 81.40.Wx

1. Introduction

Intergranular stress corrosion cracking (IGSCC) of structural materials is one of the most important problems related to aging of nuclear power plants. Among others, irradiation assisted stress corrosion cracking (IASCC) of core internals is one of the largest concerns, and it is urgently required to develop countermeasures against SCC of stainless steel materials in core of BWR.

It is known that IGSCC of stainless steels takes place only when three factors, that is, material, stress and environmental factors overlap simultaneously. Electrochemical corrosion potential (ECP) is an important measure representing the environmental factor for IGSCC of stainless steels in BWR

* Corresponding author. Tel./fax: +81 48 585 6876.
E-mail address: kishigur@rg7.so-net.ne.jp (K. Ishigure).

0022-3115/$ - see front matter
doi:10.1016/j.jnucmat.2005.11.011

condition, and it is established that there is no generation of IGSCC in the circumstance where ECP of stainless steel is maintained to be lower or baser than −230 mV.

Radiolysis of coolant water largely controls ECP of stainless steel in reactor core of BWR. The concentrations of the radiolysis products and, consequently, the values of ECP differ largely in reactor water, depending on the locations in the core. It is very difficult, however, to measure ECP directly at the various locations in actual reactor core. Hence, evaluation of ECP by calculation is very important from the practical point of view, and a technique is proposed by Macdonald [1] on the basis of a mixed potential model (MPM) in which ECP is determined as a crossing point between an integrated anodic polarization curve for stainless steel in the presence of reducing species such as hydrogen in high temperature water and an integrated cathodic polarization curve with the systems containing various oxidizing species.

This model was extended to calculate ECP of stainless steel under reactor condition of BWR [2]. The first step in this modeling is the calculation of steady state concentrations of the radiolysis products such as hydrogen, oxygen and hydrogen peroxide under irradiation by a computer code. An anodic polarization curve for stainless steel oxidation in high temperature water is given by an empirical equation based on the experiment [3], while anodic polarization curves are calculated theoretically for the surface reactions of the reducing species, for instance, hydrogen, using their steady state concentrations. They are integrated to one anodic polarization curve. Finally, an integrated polarization curve for cathodic reactions is calculated according to the similar procedure for the major oxidizing species such as oxygen and hydrogen peroxide produced by water radiolysis.

One of the important parameters required for the calculation of the polarization curves is mass transfer limited currents or limiting current densities for the redox reactions of the relevant species. The experience of the ECP measurements in reactors and in laboratory loops shows that the flow rate of the circulating water has a large effect on the ECP value, which the electrode shows in the circumstance. It is considered that this flow rate effect arises from the shift of the limiting current densities caused by the flow dependent changes in the mass transfer coefficients of the relevant species in the redox reactions.

In the previous model the radiolysis of water only in bulk is taken into account for the calculation of the steady state concentrations of oxidizing species produced, which are used to calculate the equilibrium potentials of the redox reactions, the relevant exchange current densities and also limiting current densities.

There are a very few data on ECP values measured directly within pressure vessels of BWR. The data show, however, some scatters in their dependence on the concentration of the added hydrogen, depending on the location of the measurement in the reactors, and it was pointed out that the major reason for this is due to the difference in the limiting current densities caused by the difference in the flow rates at the locations [3].

In this paper, it is shown that radiolysis of water in the diffusion layer at the interface between stainless steel and bulk water affects the limiting current densities for the anodic and cathodic reactions, and the detailed analysis is given below.

2. Calculation

2.1. Radiolysis of water

The primary process for radiolysis of water is expressed by Eq. (1), and the primary products are known to react among themselves:

$$H_2O \rightarrow e^-_{aq}, OH, H, H_2, H_2O_2, H^+ \tag{1}$$

via 50 reactions shown in Table 1. The time dependent concentration of each product in bulk water is obtained by solving the rate equations corresponding to the 50 reactions like

$$\frac{dC}{dt} = \alpha G I_b - \left(kC^2 + \sum_i k_i C_i C - \sum_i \sum_j k_{ij} C_i C_j \right), \tag{2}$$

where G is the G value for a primary product, I_b the dose rate in bulk water, α the conversion factor, C, C_i, and C_j the bulk concentrations of the relevant species and k, k_i, and k_{ij} are the relevant rate constants related to the consumption and formation of the primary product.

The steady state concentrations of chemical species produced by water radiolysis at 280 °C were calculated using FACSIMILE code [4] under the various conditions with different dose rates of radiation. The rate constants and G values for the primary species by gamma rays and neutrons

at 280 °C used for the calculations are shown in Tables 1 and 2, respectively. Most of the data in these tables are taken from the previous literature [5,6]. It is to be noted that reactions (46) and (47) that have not been considered in the earlier modeling [6]. These two reactions, especially reaction (46), were shown to give a large impact to the calculation results [5]. The rate constant of the former reaction in gas phase at high temperatures has recently been measured [7–10] and also calculated theoretically, but data in aqueous phase are not available so far. The value for this reaction given in Table 1 was evaluated on the basis of thermodynamic equilibrium, considering the rate constants measured in gas phase.

Table 1
Rate constants of elementary reactions involved in water radiolysis at 280 °C

Number	Reactions	Rate constants ($dm^3\ mol^{-1}\ s^{-1}$)
1	$OH + OH \rightarrow H_2O_2$	2.8E10
2	$OH + e^-_{aq} \rightarrow OH^-$	3.5E11
3	$OH + H \rightarrow H_2O$	2.3E11
4	$OH + O^- \rightarrow HO_2^-$	2.9E11
5	$OH + HO_2 \rightarrow H_2O + O_2$	7.6E10
6	$OH + O_2^- \rightarrow OH^- + O_2$	3.1E11
7	$OH + O_3^- \rightarrow HO_2 + O_2^-$	1.4E11
8	$OH + H_2O_2 \rightarrow H_2O + O_2^- + H^+$	4.3E8
9	$OH + HO_2^- \rightarrow H_2O + O_2^-$	8.6E10
10	$OH + H_2 \rightarrow H_2O + H$	8.9E8
11	$2\ e^-_{aq} + 2H_2O \rightarrow H_2 + 2OH^-$	3.0E6
12	$e^-_{aq} + H + H_2O \rightarrow H_2 + OH^-$	1.1E10
13	$e^-_{aq} + O^- + H_2O \rightarrow 2OH^-$	8.6E9
14	$e^-_{aq} + O_2^- + H_2O \rightarrow HO_2^- + OH^-$	3.4E9
15	$e^-_{aq} + H_2O_2 \rightarrow OH + OH^-$	2.3E11
16	$e^-_{aq} + HO_2^- \rightarrow O^- + OH^-$	4.0E10
17	$e^-_{aq} + H^+ \rightarrow H$	4.9E11
18	$e^-_{aq} + O_2 \rightarrow O_2^-$	2.2E11
19	$2H \rightarrow H_2$	9.2E10
20	$H + HO_2 \rightarrow H_2O_2$	1.6E11
21	$H + O_2^- \rightarrow HO_2^-$	2.3E11
22	$H + H_2O_2 \rightarrow H_2O + OH$	3.5E9
23	$H + OH^- \rightarrow e^-_{aq} + H_2O$	2.6E8
24	$H + O_2 \rightarrow O_2^- + H^+$	2.5E11
25	$H + O^- \rightarrow OH^-$	3.2E11
26	$2O^- + 2H_2O \rightarrow H_2O_2 + 2OH^-$	1.3E6
27	$O^- + O_2^- + H_2O \rightarrow O_2 + 2OH^-$	2.4E9
28	$O^- + O_3^- \rightarrow 2O_2^-$	1.1E10
29	$O^- + H_2O_2 \rightarrow O_2^- + H_2O$	8.1E9
30	$O^- + HO_2^- \rightarrow OH^- + O_2^-$	6.5E9
31	$O^- + O_2 \rightarrow O_3^-$	4.6E10
32	$O^- + H_2 \rightarrow H + OH^-$	1.3E9
33	$2HO_2 \rightarrow H_2O_2 + O_2$	4.5E7
34	$HO_2 + O_2^- \rightarrow O_2 + HO_2^-$	4.2E8
35	$O_3^- \rightarrow O^- + O_2$	3.45E4
36	$O_3^- + H^+ \rightarrow OH + O_2$	8.4E11
37	$H_2O_2 \rightarrow H^+ + HO_2^-$	0.46
38	$H^+ + HO_2^- \rightarrow H_2O_2$	2.56E11
39	$H_2O \rightarrow H^+ + OH^-$	4.5
40	$H^+ + OH^- \rightarrow H_2O$	1.74E12
41	$OH + OH^- \rightarrow O^- + H_2O$	1.4E11
42	$O^- + H_2O \rightarrow OH^- + OH$	6.7E7
43	$HO_2 \rightarrow H^+ + O_2^-$	1.9E6
44	$H^+ + O_2^- \rightarrow HO_2$	6.1E11
45	$e^-_{aq} + H_2O \rightarrow H + OH^-$	7.2E2
46	$H + H_2O \rightarrow H_2 + OH$	3.9E3
47	$H \rightarrow e^-_{aq} + H^+$	2.2E5
48	$e^-_{aq} + HO_2 \rightarrow HO_2^-$	2.9E11
49	$H_2O_2 \rightarrow 2OH$	2.3E−2
50	$2O_2^- + H^+ \rightarrow HO_2^- + O_2$	4.3E11

Table 2
G values for primary species of water radiolysis at 280 °C

Species	Gamma rays	Neutrons
e^-_{aq}	3.54	0.68
H	0.94	0.52
OH	3.48	1.52
H_2	1.56	1.66
H_2O_2	1.06	1.29
H^+	3.54	0.68

The steady state concentration of each species corresponding to $dC/dt = 0$ in Eq. (2) was obtained from the flat part of the time profile of each product concentration.

2.2. Polarization curves of redox reactions

ECP is calculated in MPM as a crossing point between anodic and cathodic polarization curves. According to Macdonald an empirical equation is derived for anodic polarization of stainless steel oxidation on the basis of experimental measurements, while anodic and cathodic polarization curves of redox species are calculated using Butler–Volmer equation (3) in relation to the redox reaction (4) on the surface of the stainless steel

$$i_{R/O} = \frac{e^{(E-E_{R/O})/b_a} - e^{-(E-E_{R/O})/b_c}}{\dfrac{1}{i_{o,R/O}} + \dfrac{e^{(E-E_{R/O})/b_a}}{i_{l,a}} - \dfrac{e^{-(E-E_{R/O})/b_c}}{i_{l,c}}}, \tag{3}$$

$$O + ne = R. \tag{4}$$

Here E is the potential of electrode, $E_{R/O}$ the equilibrium potential for redox reaction (4), $i_{o,R/O}$ the exchange current density, $i_{l,a}$ and $i_{l,c}$ the mass-transfer limited current densities or limiting current densities for anodic and cathodic reactions, respectively, and b_a and b_c the respective Tafel constants.

In this paper some anodic and cathodic polarization curves were calculated for the purpose of comparison using the Macdonald's procedure [3].

3. Modeling on limiting current density under irradiation

It is common in the calculation of limiting current density for a redox reaction (4) to assume the presence of a diffusion layer at the interface between a metal electrode and bulk of aqueous phase and to relate the linear diffusion rate of a redox species in the diffusion layer to the limiting current density. Thus, the limiting current density i_l for one of the redox couples is given by

$$i_l = nFDC_b/\delta, \tag{5}$$

where F refers to Faraday constant, D and C_b the diffusion constant and the steady state bulk concentration of the redox species, respectively, and δ is the thickness of the diffusion layer.

In the previous MPM for the system under irradiation, the radiolysis products, H_2O_2, O_2 and H_2, are taken into account for the redox reactions and their bulk concentrations, C_b, are calculated using a computer code and δ is evaluated from a mass-transfer coefficient using an empirical equation. Several equations are proposed for the calculation of δ under the various conditions in the field of chemical engineering. One of the examples with the high flow rate of water passing through a channel is given by [3]

$$\delta = d/(0.0165Re^{0.86}Sc^{0.33}). \tag{6}$$

Here Re is Reynolds number, Sc the Schmidt number and d is the channel diameter.

The water radiolysis, however, produces the same species not only in the bulk water but also in the diffusion layer, affecting the concentration profiles of the species in the diffusion layer. This effect may be taken into account in the calculation of the limiting current densities of the redox reactions, and is modeled as follows.

For simplicity one dimensional model is considered. As shown in Fig. 1, a diffusion layer with thickness δ is assumed to exist at the interface between the metal surface and the bulk water under irradiation. The concentration of a radiolysis product, c, at position x in the diffusion layer is approximated by

$$\frac{\partial c}{\partial t} = \alpha GI + \left(\frac{\partial^2 c}{\partial x^2}\right)D - \left(kc^2 + \left(\sum_i k_i c_i\right)c - \sum_i \sum_j k_{ij}c_i c_j\right). \tag{7}$$

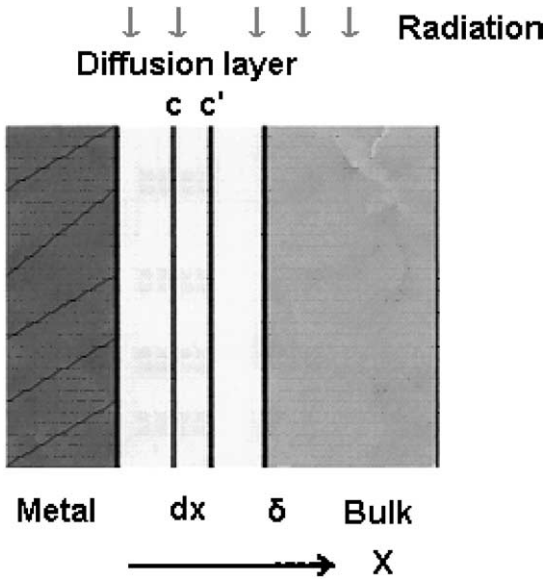

Fig. 1. Schematic diagram of diffusion layer at the interface between metal electrode and bulk water.

Here I is a dose rate of radiation in the diffusion layer, c_i the concentration of the other species i at the position x in the diffusion layer, and k, k_i and k_{ij} the rate constants for the relevant reactions of the species. Considering the steady state, Eq. (7) is rearranged into Eq. (8) and the integration of Eq. (8) gives Eq. (9) using the assumed average concentrations, $\underline{c_i}$ and $\underline{c_j}$ and, the assumed constant dose rate I in the diffusion layer:

$$\frac{d^2c}{dx^2} = -\frac{\alpha GI}{D} + \left(\frac{k}{D}\right)c^2 + \sum_i \left(\frac{k_i c_i}{D}\right)c - \sum_i \sum_j \frac{k_{ij}c_i c_j}{D}, \tag{8}$$

$$\frac{dc}{dx} = \left[2A - \left(\frac{2\alpha GI}{D}\right)c + \left(\frac{2k}{3D}\right)c^3 + \left(\sum_i \frac{k_i \underline{c_i}}{D}\right)c^2 - \left(2\sum_i \sum_j k_{ij}\frac{\underline{c_j}\,\underline{c_j}}{D}\right)c\right]^{1/2}, \tag{9}$$

where A is an integration constant. Eq. (10) is derived under the boundary condition $c = 0$ at $x = 0$

$$(dc/dx)_{x=0} = (2A)^{1/2}. \tag{10}$$

Consideration of the mass balance with the diffusion layer gives Eq. (11), if Eq. (12) is assumed to hold in relation to Eq. (8) when t is small for the diffusion of the species inside the diffusion layer. Solving the equations for A finally gives Eq. (13):

$$\left(\frac{dc}{dx}\right)_{x=\delta} = \left[2A - \frac{2\alpha GIC_b}{D}\right]^{1/2}, \tag{11}$$

$$kc^2 + \left(\sum_i k_i c_i\right)c - \sum_i \sum_j k_{ij} c_i c_j = 0, \tag{12}$$

$$(2A)^{1/2} = \frac{C_b}{\delta} + \frac{\alpha GI\delta}{2D}. \tag{13}$$

Now the ratio f of the limiting current density $i_l(I)$ with the consideration of the irradiation in the diffusion layer at a dose rate I to that without the consideration of the irradiation, $i_l(0)$, is written as

$$f = \frac{i_l(I)}{i_l(0)} = 1 + \frac{\alpha GI\delta^2}{2DC_b}. \tag{14}$$

The last term in Eq. (14) is added with the consideration of the irradiation in the diffusion layer, and dependent on the dose rate, the flow rate and also water chemistry.

4. Results and discussion

4.1. Validity of approximation

In the above analysis Eq. (12) was assumed to approximately hold in the diffusion layer if the diffusion time t_d is small. Eq. (12) claims that the chemical reaction terms in Eq. (7) of the relevant species cancel each other between its formation and consumption during the short diffusion time after it enters the diffusion layer from the bulk with its steady state concentration C_b. The diffusion time t_d is approximately evaluated by means of Einstein–Smoluchowsky equation

$$\langle l^2 \rangle = 2Dt_d, \tag{15}$$

where l is the diffusion distance. If l is taken to be δ, t_d is readily calculated for hydrogen peroxide as shown in Table 3.

In Fig. 2 are shown typical examples for the calculated time profiles of the concentrations of the chemical species after the irradiation is stopped in the steady state. In this condition the concentrations of the chemical species are determined by Eq. (16) with each initial value of the steady state concentration of the species since the dose rate is set to be zero in Eq. (2):

$$\frac{dC}{dt} = -\left[kC^2 + \left(\sum_i k_i C_i\right)C - \sum_i \sum_j k_{ij} C_i C_j\right]. \tag{16}$$

It is evident from this figure that the concentrations of H_2O_2 and H_2 are almost constant at least up to 0.1 s after stopping the irradiation, whereas the other species like OH, HO_2, O_2^-, and e_{aq}^- decay more rapidly. When the dose rate was changed in the calculation, the steady state concentrations of the relevant species varied correspondingly, but the time dependence was very similar to those in

Table 3
Examples of calculated diffusion time with changing flow rate

Flow rate ($m\ s^{-1}$)	Diffusion time, t_d (s)
0.3	8.8×10^{-2}
0.6	2.8×10^{-2}
2	3.4×10^{-3}
3	1.7×10^{-3}

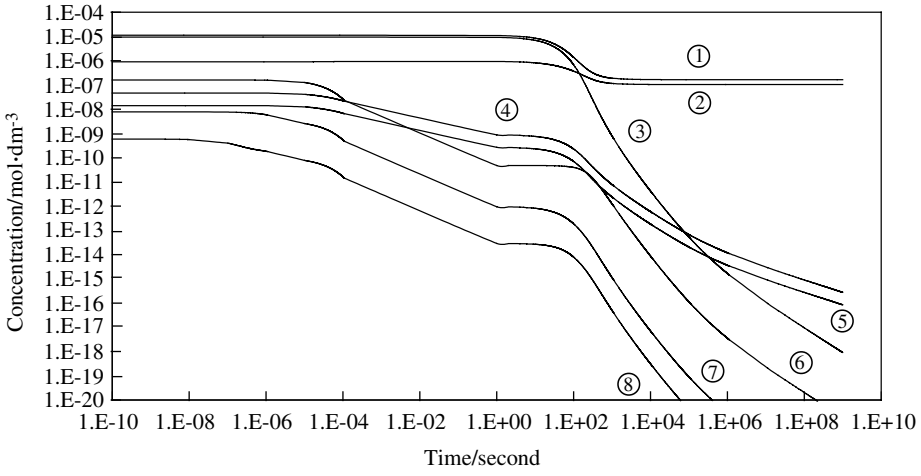

Fig. 2. Calculated time profiles of the concentrations of the radiolysis products after the irradiation is stopped in the steady state. Gamma rays, dose rate 1×10^4 Gy s^{-1}; (1) H_2, (2) O_2, (3) H_2O_2, (4) HO_2, (5) O_2, (6) OH, (7) H, (8) e_{aq}^-.

Fig. 2 with the constant concentrations of H_2O_2 and H_2 up to 0.1 s or longer. Thus it may be concluded that the approximation used in the above analysis is applicable with reasonable accuracy to the species, H_2O_2 and H_2, but should be carefully applied to the other species.

4.2. Profiles of concentration in the diffusion layer

Integration of Eq. (8) under the condition of Eq. (12) gives readily the profiles of the concentration of relevant species in the diffusion layer. Some examples of the calculated profiles are shown in Fig. 3 for hydrogen peroxide under the various dose rates. In the area where x is near δ in the diffusion layer, the diffusion rate term in Eq. (7) is comparatively small, especially, when the dose rate is high and, consequently, negligible. Thus, the concentrations of H_2O_2 in this area are very close to the steady state concentrations in the bulk water.

The diffusion rate of the species at the surface of the stainless steel is determined by the concentration gradient therein given by Eqs. (10) and (13), and is seen in Fig. 3 to be larger at the higher dose rates than the linear slope calculated without the consideration of the irradiation in the diffusion layer.

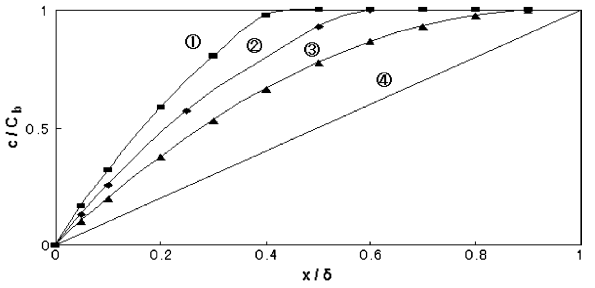

Fig. 3. Profiles of H_2O_2 concentrations in the diffusion layer. Gamma rays, flow rate 0.59 m s^{-1}; dose rate (1) 1×10^4 Gy s^{-1} (HWC), (2) 1×10^4 Gy s^{-1} (no additive), (3) 1×10^3 Gy s^{-1} (HWC), (4) irradiation in the diffusion layer not considered.

It is known that the absorbed doses of radiation increases in a thin water layer contacting with a metal surface compared to those in bulk owing to the back scattering of the radiation, but the increment is 10–20% of the absorbed dose in bulk in case of the water layer contacting with usual metal like Fe or Ni [11]. In the present calculation, it was assumed that the absorbed doses are the same between the interface thin layer and the bulk of water.

4.3. Effect of dose rate

As mentioned above, f-factor defined by Eq. (14) depends on the various parameters of the environmental conditions. In Table 4 the values of the f-factor are shown for H_2O_2 and H_2 in the conditions of simulated normal water chemistry (NWC) with initial dissolved oxygen (DO) = 200 ppb and simulated hydrogen water chemistry (HWC) with initial dissolved hydrogen (DH) = 50 ppb and DO = 10 ppb for various dose rates of gamma irradiation. It is evident that the f-values increase significantly with increasing dose rate to the in-core level, while it is negligible at the lower dose rate levels of laboratory experiments. Their increments are larger for H_2O_2 than for H_2 owing to the larger G value of the former under the gamma irradiation. It is also seen in Table 4 that the f-factors for H_2O_2 are larger with the HWC condition than with the NWC condition at the same dose rate, whereas those for H_2 are smaller with the HWC condition than with the NWC condition.

In Table 5 are shown the values of the f-factor for neutron irradiation in the simulated NWC and HWC conditions with various dose rates. As already shown in Table 2 the G values for H_2O_2 and H_2 are significantly larger with neutrons than with gamma rays. However, the f-factor for H_2O_2 is smaller with neutrons than those with gamma rays at the same dose rates in the NWC condition.

Table 4
Effect of dose rate on f-factor for H_2O_2 and H_2 by gamma irradiation 280 °C, flow rate 0.59 m s^{-1}

Chemistry	Chemical species	Dose rate (Gy s^{-1})					
		1×10^4	7×10^3	3×10^3	1×10^3	1×10^2	1
NWC	$f(H_2O_2)$	2.71	2.27	1.64	1.25	1.03	1.01
	$f(H_2)$	2.10	1.87	1.49	1.23	1.04	1.00
HWC	$f(H_2O_2)$	5.40	4.84	3.15	2.15	1.34	1.03
	$f(H_2)$	1.52	1.39	1.19	1.04	1.005	1.000

NWC: initial DO = 200 ppb, HWC: initial DO = 10 ppb, DH = 50 ppb.

Table 5
Effect of dose rate on f-factor for H_2O_2 and H_2 by neutron irradiation 280 °C, flow rate 0.59 m s^{-1}

Chemistry	Chemical species	Dose rate (Gy s^{-1})					
		1×10^4	7×10^3	3×10^3	1×10^3	1×10^2	1
NWC	$f(H_2O_2)$	1.48	1.36	1.18	1.007	1.001	1.001
	$f(H_2)$	1.67	1.52	1.26	1.12	1.02	1.002
HWC	$f(H_2O_2)$	2.56	2.36	2.00	1.64	1.23	1.03
	$f(H_2)$	1.95	1.75	1.39	1.16	1.02	1.000

This arises from the fact that the steady state concentration C_b of H_2O_2 in bulk increases owing to the higher G value for neutrons and this masks the effect of the increased G values in the second term of Eq. (14). Similarly, the f-factor for H_2 is smaller with the neutrons than with the gamma rays in the NWC condition due to the same reason for H_2O_2.

On the other hand, the f-factor for H_2 in the HWC condition is larger with the neutrons than with the gamma rays, since in the HWC condition the bulk concentration of H_2 is mainly controlled by the large concentration of added H_2.

4.4. Effect of water chemistry

As seen in the previous section, the f-factor is affected largely by water chemistry, especially, by H_2 addition. In Fig. 4 the f-factor for H_2O_2 are plotted with changing concentrations of DH at the different dose rates of gamma rays when the initial concentration of DO is fixed at 200 ppb. It is very clear that the f-factor increases with increasing DH and this effect is enhanced at the higher dose rates of the gamma irradiation. The increase in the f-factor with increasing DH is due to the decrease in the bulk concentration of hydrogen peroxide. For example, the bulk concentrations of H_2O_2 calculated are 6.69×10^{-6} mol dm^{-3} and 8.89×10^{-7} mol dm^{-3} for 50 ppb and 400 ppb of DH, respectively, at the dose rate of 1×10^4 Gy s^{-1}. At the lower dose rate of 1×10^3 Gy s^{-1} the bulk concentrations of hydrogen peroxide are lower than those at the higher dose rate, which pushes up the f-factor, while the dose rate effect decreases the f-factor. The total effect, however, leads to the lower f-factor at the lower dose rate.

4.5. Effect of flow rate

Flow rate is another important element affecting the f-factor through the thickness (δ) of the diffusion layer that is determined by the mass transfer coefficient of the system. In Fig. 5 the f-factor for H_2O_2 is plotted with changing flow rates at the dose rate of 1×10^4 Gy s^{-1} of gamma rays in the NWC and HWC conditions. As seen from the figure the f-factor decrease sharply with increasing flow rate and approach the value of 1 where the irradiation effect in the diffusion layer is negligible. The high flow rate decreases the thickness of the diffusion layer, δ, and, consequently, gives the steep concentration gradient (C_b/δ) of the species, for example,

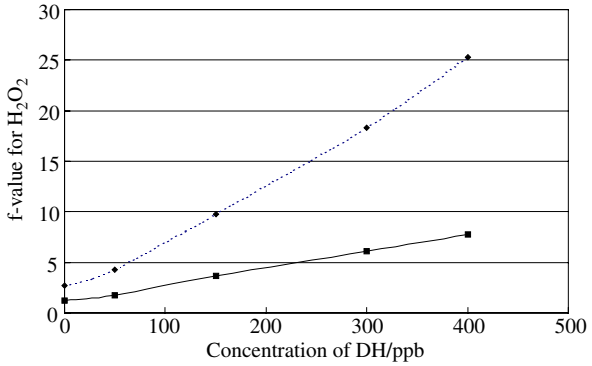

Fig. 4. Effect of dissolved hydrogen concentration on f-factor for H_2O_2. (···◆···) 1×10^4 Gy s^{-1}, (–■–) 1×10^3 Gy s^{-1}, gamma rays, flow rate 0.59 m s^{-1}, initial DO = 200 ppb.

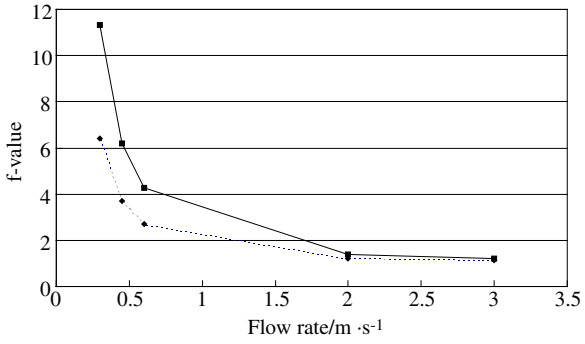

Fig. 5. Effect of flow rate on f-factor for H_2O_2 in the simulated NWC and HWC conditions. (–■–) HWC (initial DH = 50 ppb, DO = 10 ppb), (···◆···) NWC (initial DO = 200 ppb), gamma rays, 1×10^4 Gy s^{-1}, flow rate 0.59 m s^{-1}.

hydrogen peroxide in the diffusion layer even when the irradiation effect in the diffusion layer is not taken into account. Thus, the high flow rate leads to the larger $I_l(0)$ and consequently, to the lower f-factor.

It is to be noted that in principle the f-factor increases further at the much lower flow rates than those shown in Fig. 5, but in such the condition the mass transfer coefficient may be derived on the basis of the equation different from Eq. (6). Also the increased δ leads to the longer diffusion time and in that case the approximation used in this analysis may not be appropriate to be applied.

Another point to be mentioned is the effect of the channel diameter (d) on the thickness of the diffusions layer, δ. In the above analysis d is fixed to be 2.3 cm for comparison. If d is decreased independently of flow rate, then the f-factor is also decreased because of the decrease in δ in Eq. (14). For instance, if d is decreased from 2.3 cm to 0.8 cm, the f-factor for H_2O_2 in the HWC condition are reduced to 4.27 and 3.63 at the dose rates of 1×10^4 Gy s^{-1} and 7×10^3 Gy s^{-1}, respectively. In the actual case the flow rate is more or less related to the channel diameter, not being independent of it.

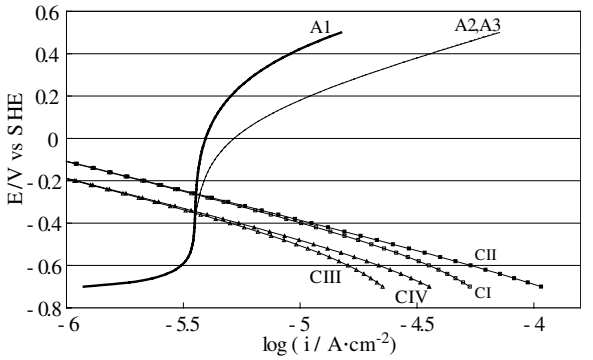

Fig. 6. Anodic and cathodic polarization curves calculated using parameters in literature [12,13] in the simulated HWC condition (initial DH = 50 and DO = 10 ppb). A1: Anodic polarization (DH = 0) of stainless steel oxidation. A2: Anodic polarization with the HWC, irradiation in the diffusion layer not considered ($f = 1$). A3: Anodic polarization with the HWC, gamma irradiation (1×10^4 Gy s^{-1}) in the diffusion layer considered ($f = 1.52$). CI: cathodic polarization for H_2O_2 with HWC, irradiation in the diffusion layer not considered ($f = 1$). CII: Cathodic polarization for H_2O_2 with HWC, gamma irradiation (1×10^4 Gy s^{-1}) in the diffusion layer considered ($f = 5.4$). CIII: cathodic polarization for H_2O_2 with the HWC, irradiation in the diffusion layer not considered ($f = 1$). CIV: cathodic polarization for H_2O_2 with the HWC, gamma irradiation (1×10^3 Gy s^{-1}) in the diffusion layer considered ($f = 2.15$).

5. Model calculation of polarization curves

The above analysis is concentrated on the effect of the several parameters on the f-factor, and in this section a model calculation is carried out on the effect of the f-factor on polarization curves. As described previously, the f-factor for H_2O_2 is more increased in the simulated HWC conditions, and, thus, the model calculations of cathodic and anodic polarization curves were performed for the simulated HWC conditions and compared between the cases with and without the consideration of the irradiation in the diffusion layer.

Input parameters, exchange current densities and Tafel constants, are required to calculate the polarization curves for redox reactions of hydrogen and hydrogen peroxide. These data are given in literature [3], but the data reported recently [12,13] are somewhat different from the previous ones. There is some uncertainty on these parameters and therefore the calculations of the polarization curves were carried out for comparison using the two sets of the parameters, ones from literature [3] and the others from the recent papers [12,13].

In Fig. 6 are shown the polarization curves calculated using the recent parameters in the literature [12,13] for the redox reactions of hydrogen and hydrogen peroxide. Curve A1 is a typical anodic polarization curve of the stainless steel oxidation in pure water at 280 °C that was derived from adjusting the empirical equation given by Macdonald to experimental results. Curves A2 and A3 are the integrated anodic polarization curves including the anodic reaction of hydrogen in the simulated HWC condition. Curves A2 and A3 were corresponding to $f = 1$ without, and $f = 1.52$ with, the consideration of the gamma irradiation of dose rate 1×10^4 Gy s^{-1} in the diffusion layer, but there is no significant difference in this potential area between these polarization curves.

Curves CI and CII are the cathodic polarization curves of hydrogen peroxide calculated in the same HWC condition, CI and CII being corresponding to $f = 1$ and $f = 5.4$, respectively. It is seen that the increase in the f-factor for H_2O_2 gives a small effect on the ECP value calculated in this condition. The difference is less than 10 mV between the cases with and without the consideration of the irradiation in the diffusion layer, and almost negligible.

Curves CIII and CIV are the cathodic polarization curves of hydrogen peroxide in the same

HWC condition but with the lower gamma dose rate of 1×10^3 Gy s^{-1}. Again the difference in ECP is very small (10 mV) when calculated in this condition.

In Fig. 7 are shown the anodic and cathodic polarization curves under the simulated HWC condition with initial DH = 600 ppb and DH = 200 ppb. Curve A4 is the anodic polarization curve including the anodic reaction of H_2 in this condition. The irradiation in the diffusion layer does not give significant effect on the *f*-factor for H_2 owing to the high concentration of H_2 in bulk in this condition. Curves CV and CVI are the cathodic polarization curves for H_2O_2 calculated using the same recent parameters in the same HWC condition. The former is corresponding to $f = 1$ and the latter $f = 10.3$. It is seen in Fig. 7 that there is a significant difference, about 100 mV, in the ECP values determined between the two cases with and without the consideration of the irradiation in the diffusion layer.

The same calculations of the polarization curves were carried out using the previous parameters in literature [3] in the same HWC conditions, and the results give the larger differences in ECP values between the cases with and without the consideration of the irradiation in the diffusion layer. For example, the differences are approximately 50 mV between corresponding CI and CII, 40 mV between CIII and CIV, and 260 mV between CV and CVI.

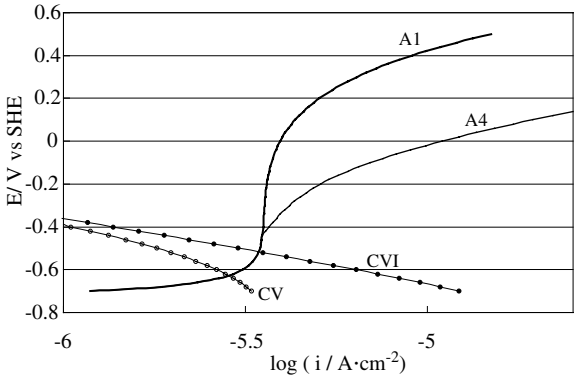

Fig. 7. Anodic and cathodic polarization curves calculated using the same parameters as in Fig. 6 in the strong HWC condition (initial DH = 600 ppb and DO = 200 ppb). A1: The same as in Fig. 6. A4: Anodic polarization with the strong HWC no significant difference in this area of the electric potential between the cases with and without the gamma irradiation (1×10^3 Gy s^{-1}). CV: Cathodic polarization for H_2O_2, irradiation in the diffusion layer not considered ($f = 1$). CVI: Cathodic polarization for H_2O_2, irradiation gamma irradiation (1×10^3 Gy s^{-1}) in the diffusion layer considered ($f = 10.3$).

Thus, the effect of the water radiolysis in the diffusion layer on the ECP evaluation is not negligible in some cases of HWC condition, depending on the environmental conditions determined by dose rate, flow rater and water chemistry. For instance, the *f*-factor is larger at the higher dose rates and at the lower flow rates. However, it is to be noted that the calculated ECP values are also affected by the shape of the corresponding anodic polarization curves derived from the oxidation of stainless steel and the anodic reaction of hydrogen as shown in Figs. 6 and 7.

6. Conclusions

The effect of water radiolysis in the diffusion layer at the interface between stainless steel electrode and bulk water was analyzed and modeled in relation to the evaluation of ECP of the stainless steel in high temperature water under irradiation. A simple approximation method was applied in the model to hydrogen peroxide and hydrogen among the radiolysis products. It was shown that the water radiolysis gives the some change in the profile of the concentration of the species in the diffusion layer in comparison with the previous model in which the radiolysis in the diffusion layer is neglected and, consequently, affects the diffusion limited current or the limiting current densities for anodic and cathodic reactions of the species. This radiolysis effect was found to depend largely on the several factors of the system such as dose rate, flow rate and water chemistry, and significantly increases the limiting current densities in some conditions.

Model calculation of anodic and cathodic polarization curves shows that this radiolysis effect affects significantly the values of ECP in some conditions of HWC.

Acknowledgement

This work was supported by a Grant-in-Aid for Scientific Research [(B)14,380,238] of the Ministry of Education, Culture, Science and Technology of Japan.

References

[1] D.D. Macdonald, M.U. Macdonald, Corros. Sci. 32 (1991) 51.
[2] T.K. Yeh, D.D. Macdonald, A.T. Motta, Nucl. Sci. Eng. 121 (1995) 468.

[3] D.D. Macdonald, Corrosion 48 (3) (1992) 194.
[4] E.M. Chance, A.R. Curtis, I.P. Jones, C.R. Kirby, AERE-R8775, 1997, AERE, Harwell.
[5] G.R. Sunaryo, Y. Katsumura, K. Ishigure, Radiat. Phys. Chem. 45 (1995) 703.
[6] K. Ishigure, J. Takagi, H. Shiraishi, Radiat. Phys. Chem. 29 (1987) 195.
[7] S. Madronich, W. Felder, J. Phys. Chem. 88 (1984) 1857.
[8] J.V. Michael, J.W. Sutherland, J. Phys. Chem. 92 (1998) 2853.
[9] M.J. Bronikowski, W.R. Simpson, R.N. Zare, J. Phys. Chem. 97 (1993) 2194.
[10] T.N. Truong, T.J. Evans, J. Phys. Chem. 98 (1994) 9558.
[11] J. Dutreix, M. Bernald, Brit. J. Radiol. 39 (1996) 205.
[12] T.K. Yeh, in: Proc. 5th Intern. Workshop on LWR Coolant Water Radiolysis and Electrochemistry, San Francisco, 2004.
[13] T.K. Yeh, in: Proc. Symps. on Water Chemistry and Corrosion of Nuclear Power Plants in Asia, Gyeongju, 2005, p. 167.